DEVELOPMENT OF MECHANICAL CHARACTERIZATION METHOD OF HYDROGEL SCAFFOLDS USING SYNCHROTRON PROPAGATION-BASED IMAGING

A Thesis Submitted to the

College of Graduate and Postdoctoral Studies

in Partial Fulfillment of the Requirements

for the Degree of Master of Science

in the Division of Biomedical Engineering

University of Saskatchewan

Saskatoon.

By

Naitao Li.

PERMISSION TO USE

In presenting this thesis in partial fulfillment of the requirements for a Master of Science degree from the University of Saskatchewan, I agree that the Libraries of this University may make it freely available for inspection. I further agree that permission for copying of this thesis in any manner, in whole or in part, for scholarly purposes may be granted by Dr. Daniel Chen and Dr. Ning Zhu who supervised my thesis work or, in their absence, by the Head of the Department or the Dean of the College in which my thesis work was done. It is understood that any copying or publication or use of this thesis or parts thereof for financial gain shall not be allowed without my written permission. It is also understood that due recognition shall be given to me and to the University of Saskatchewan in any scholarly use, which may be made of any material in my thesis.

Requests for permission to copy or to make other uses of materials in this thesis/dissertation in whole or part should be addressed to:

Head of the Division of Biomedical Engineering
57 Campus Drive, University of Saskatchewan
Saskatoon, Saskatchewan S7N 5A9
Canada.

OR

Dean
College of Graduate and Postdoctoral Studies
University of Saskatchewan
116 Thorvaldson Building, 110 Science Place
Saskatoon, Saskatchewan S7N 5C9
Canada.

DISCLAIMER STATEMENT

Here by I declare that this thesis has been composed solely by myself and that it has not been submitted, in whole or in part, in any previous application for a degree. Except where stated otherwise by reference or acknowledgment, the work presented is entirely my own.

Naitao Li. Oct 2023.

ABSTRACT

Hydrogel-based scaffolds have been widely used in soft tissue regeneration due to their biocompatible and tissue-like environment for maintaining cellular functions and tissue regeneration. Understanding the mechanical properties and internal microstructure of hydrogel-based scaffold, once implanted, is imperative in many tissue engineering applications and longitude studies. Notably, this has been challenging to date as various conventional characterization methods by, for example, mechanical testing (for mechanical properties) and microscope (for internal microstructure) are destructive as they require removing scaffolds from the implantation site and processing samples for characterization. Synchrotron propagation-based imaging – computed tomography (PBI-CT) is feasible and promising for non-destructive monitoring of hydrogel scaffolds. As inspired, this study aimed to perform a study on the characterization of mechanical properties and microstructure of hydrogel scaffolds based on the PBI-CT.

The hydrogel solutions were prepared from 3% w/v alginate + 1% w/v gelatin and then printed by using the needle with a diameter of 200 μm, to form scaffolds with a dimension of 10×10×5 mm^3. After successfully crosslinking of scaffolds, some of the scaffolds were degraded in a 37 °C media of phosphate buffered saline over 3 days, for the subsequent examination, along with those without degradation. The scaffolds both with and without degradation were subject to compressive testing, where the compression speed was set at 0.1 mm/s to reach the strain of 10%, 20%, 30%, 40%, and 50%, respectively. Once reached, the strain was held for 5 minutes for measuring the force and thus the stress within scaffolds, yielding the stress–strain curves. After that, the scaffolds were imaged and examined by SR-PBI-CT at the BMIT-ID beamline at Canadian Light Source (CLS). During the imaging process, the scaffolds were mechanically loaded, respectively, with the strains same as the ones in the aforementioned compressive testing, and at each strain, the scaffold was imaged and scanned with a pixel size of 13 μm for analysis.

From the stress-strain curves obtained in the compression testing, the Young's modulus was evaluated to characterize the elastic behavior of scaffolds: with the range between around 5-25 kPa; from the images captured by SR-PBI-CT, the scaffolds microstructures were examined in terms of

the strand cross-section area, pore size, and hydrogel volume. Further, from the SR-PBI-CT images, the stress within hydrogel of scaffolds were evaluated, showing the agreement with those obtained from compression testing. These results have illustrated that the mechanical properties and microstructures of scaffolds, ether being degraded or not, can be examined and characterized by the SR-PBI-CT imaging, in a non-destructive manner. This would represent a significant advance for facilitating longitude studies on the scaffolds once implanted *in-vivo*.

ACKNOLEDGEMENTS

I would like to express my sincere and deepest gratitude to my supervisors, Dr. Daniel Chen and Dr. Ning Zhu, for their great support, encouragement, and guidance during my academic studies and research. They have been a great source of knowledge and inspired me to pursue this research. I would like to thank my advisory committee members, Dr. Emily McWalter, and Dr. Tate Cao, for their valuable comments and suggestions.

It is acknowledged that this study was supported by the Natural Sciences and Engineering Research Council of Canada (NSERC). Imaging, reconstruction, and segmentation parts of research described in this paper were performed at the Canadian Light Source, which is a national research facility supported by the Canada Foundation for Innovation (CFI), NSERC, National Research Council (NRC), Canadian Institutes of Health Research (CIHR), Government of Saskatchewan, and the University of Saskatchewan.

I would like to thank Ms. Farinaz Ketabat, Mr. Reza Gharraei and Dr. Zahra Yazdanpanah for their committed tutoring of bio-fabrication related experiments. The technical support from Mr. Doug Bitner is highly appreciated. I also appreciate Ms. Xiaoman Duan and Mr. Xiaofan Ding for their sincere support and collaboration throughout imaging related parts, including set-up and data processing of my academic studies. My sincere thanks to all friends from Daniel's Bio-fabrication Laboratory and Ning's Imaging Group who have been a great support during my academic studies and research. Again, I am grateful for fantastic support, encouragement, and guidance from Dr. Daniel Chen and Dr. Ning Zhu during my academic studies and research.

Finally, above all, I am grateful to my parents, Jianbin Li and Ying Zhang, for their love, patience, and motivation, as well continuous financial support for my life in Canada.

TABLE OF CONTENTS

LIST OF FIGURES

LIST OF ABBREVIATIONS

μCT: X-ray micro-computed tomography

3D: Three-dimensional

Alg-Ge: 3% alginate and 1% (w/v) gelatin biomaterial solution

BMIT: Bio-Medical Imaging and Therapy

CLS: Canadian Light Source

CT: Computed tomography

DMA: Dynamic Mechanical Analysis

ECM: Extracellular Matrix

FEA: Finite Element Analysis

MRI: Magnetic Resonance Imaging

PBI: Propagation-based Imaging

PBS: Phosphate-buffered saline

SDD: Sample-to-detector distance

SEM: Scanning electron microscope

SR-PBI: Synchrotron radiation propagation-based imaging technique

UFO: Ultra-Fast-Online software (an open-source package)

UV: Ultraviolet

CHAPTER 1. INTRODUCTION

1.1. Hydrogel Scaffolds in Tissue Engineering

Porous scaffolds play a key role in tissue engineering aimed to treat damaged tissue or organs. The scaffolds provide the essential structure and microenvironment that support cellular adhesion, proliferation, and differentiation, all of which are critical for tissue growth and maturation [1]. These scaffolds must be biodegradable, for allowing the regeneration of new tissue as the scaffolds degrade [2]. Different materials, such as bioceramics, biodegradable polymers, and hydrogel materials, are used to fabricate these scaffolds [3]. The typical process of applying scaffolds for treating damaged tissue/organs is shown in Figure 1.1, which includes the following steps: selection of appropriate growth factors, cells/ stem cells, and biomolecules, scaffold fabrication, culturing and implantation of scaffold to the body [4].

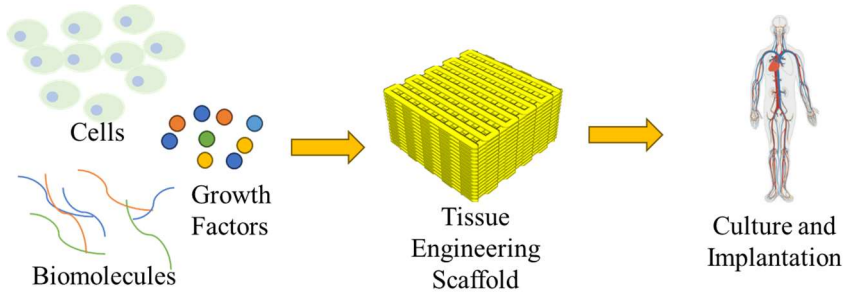

Figure 1.1. Schematic depicting the schemes in tissue regeneration by means of scaffolds, modified from [4].

Hydrogel-based materials have been widely used in the fabrication of scaffolds for soft tissue regeneration due to their superiority of providing a biocompatible, tissue-like environment for maintaining cellular functions and tissue regeneration. Hydrogel materials are able to mimic the natural extracellular matrix (ECM) with high-water content and porosity[5], appropriate mechanical properties for scaffold support, and biological properties for cell [4, 6-8]. While hydrogel-based scaffolds have been widely used for their exceptional biocompatibility but limited

by their inherent mechanical weakness and structure instability. As such, understanding the mechanical properties of hydrogel-based scaffold, particularly after implanted, becomes imperative in tissue engineering applications and longitude studies.

1.2. Mechanical Characterization of Tissue Engineering Scaffolds

Mechanical property characterization of tissue scaffolds is important for the development of scaffolds for tissue regeneration. Tissue engineering scaffolds must be strong enough to mechanically support the scaffold structure, as the scaffold material degrades and new tissue regenerates. The scaffold structure may also be changed by the forces produced by kinetic bodies, or unexpected external forces such as compression and stretching [9]. Thus, it is critical to characterize mechanical properties and internal microstructure of scaffolds [4].

Traditional approaches for assessing the mechanical properties of tissue engineering scaffolds often include those based on mechanical testing by applying compression, tensile, bending, and torsion, as shown in Figure 1.2. Compression testing involves the application of a compressive force to a scaffold sample, which allows for the measurement of compressive strength, stiffness, and deformation behavior [10]. This not only aids in determining the scaffold's ability to withstand compression but also provides invaluable data about its structural stability under various pressure conditions. On the other hand, tensile testing entails applying a tensile force to a scaffold until it fails, thereby yielding information about its tensile strength, elongation at break, and Young's modulus [11]. This method is crucial in evaluating a scaffold's capability to resist stretching forces, a key requirement considering the kinetic nature of physiological environments. Simultaneously, bending tests, which measure a scaffold's flexural characteristics and its resistance to bending forces, provide vital insights for scaffolds designed for load-bearing applications [12]. Lastly, shear/torsion tests, conducted to evaluate a scaffold's resistance to forces operating parallel to its surface, offer measures of shear strength and overall structural integrity, contributing significantly to understanding its appropriateness for various tissue engineering applications [13]. Collectively,

these methods form a robust and comprehensive strategy to evaluate the mechanical properties of tissue engineering scaffolds.

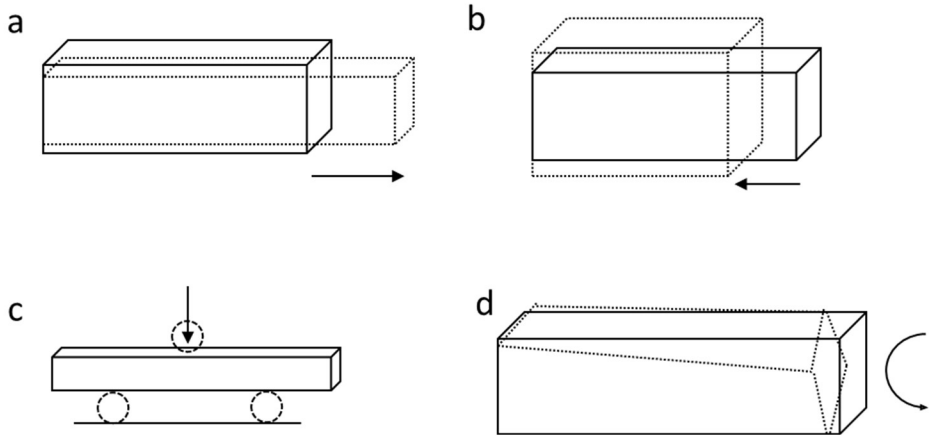

Figure 1.2. Types of loading conditions applied to a specimen: (a) tensile, (b) compressive, (c) bending, and (d) torsion, modified from [4].

In addition to the aforementioned approaches, Dynamic Mechanical Analysis (DMA) is one technique to evaluate the mechanical traits of materials under dynamic loading conditions, such as cyclic or oscillatory forces [14]. The DMA quantifies the viscoelastic characteristics of the material, presenting valuable insight into the scaffold's performance under dynamic conditions that mimic the physiological ones. This provides an effective measure to investigate the functional reliability and long-term durability of the scaffold, especially in cases where repetitive loadings are anticipated [15]. The information gleaned from these analyses helps guide the optimization of scaffold designs, materials, and fabrication methods, with an aim to engineer constructs that more closely mimic the complex, dynamic behavior of native tissues.

1.3. Visualization of Scaffold Structures

Besides the mechanical characterization, visualizing and assessing the scaffold structure such as pore size and porosity, are important and represent a critical aspect of tissue engineering, as these attributes significantly influence mechanical properties [16, 17]. Techniques such as micro-

computed tomography (μCT) and scanning electron microscopy (SEM) are instrumental in evaluating these factors, thanks to their ability to provide precise measurements and high-resolution imaging, respectively [18, 19]. There is a complex relationship between scaffold porosity and mechanical performance; for example, scaffolds with carefully balanced porosity can offer enhanced mechanical stability while also encouraging cellular proliferation and tissue regeneration [17, 20]. μCT serves as a valuable tool in this context by leveraging X-ray imaging to create detailed three-dimensional representations of the scaffold, enabling non-invasive evaluation of structural parameters [18]. Simultaneously, SEM provides a platform capable of capturing the minutiae of scaffold structures, thus proving highly effective in analyzing and measuring scaffold characteristics [19, 21]. Overall, the characterization of scaffold architecture such as pore size and porosity in tissue engineering scaffolds is crucial for understanding their mechanical behavior. Advanced imaging modalities like μCT and SEM provide comprehensive insights into these structural aspects, ultimately aiding the optimization of scaffold design and fostering improved tissue regeneration [22, 23].

Large depth visualization of scaffolds architecture is critical for analyzing the performance of scaffolds including structural, biological, mechanical properties, but conventional μCT cannot work well with low-density hydrogel material. μCT is a technique developed by computer processing with a spatial resolution up to a micrometer level ranging between 6 μm and 50 μm with the help of contrast agents and has been well develop during recent years for medical related fields. μCT is a well-built non-destructive technique with high-resolution imaging and three-dimensional visualization with voxel size up to 1 μm, which is better compared to ultrasound imaging and magnetic resonance imaging [24]. The high radiation dose for live animal imaging is a significant disadvantage in tissue engineering studies [25], meanwhile the long-time consumption for μCT scanning can eventually increase the chance of introducing motion artifact into imaging. The most critical challenge in conventional absorption-based μCT is to visualize low-density materials due to the low X-ray absorption attenuation of these materials, including hydrogel [26, 27]. It is evident that this technique is not appropriate for imaging and visualization of hydrogel scaffolds considering these discussed limitations.

Based on conventional μCT, synchrotron X-ray based CT shows significant advantage compared to conventional μCT, and SR-PBI-CT is capable of visualization and characterization of hydrogel scaffolds [27]. Synchrotron radiation is a brilliant light source producing X-rays of high photon flux and coherence, ensuring a more significant potential for the development of new imaging techniques. X-ray propagation-based imaging (PBI), which is based on the refraction of X-rays, has shown promise with respect to soft tissue visualization due to much higher refractive index variations compared to X-ray absorption coefficient variations [28]. Because of the high brightness and high coherence of synchrotron radiation (SR) source, SR-PBI imaging has shown great capability to visualize and distinguish low-density soft tissues and hydrogels with high spatial resolution and scan speed [29]. At the same time, the high imaging depth comes with X-ray CT also ensures the imaging ability of the entire scaffold [30]. Previously reported studies have confirmed that it is feasible to use SR-PBI-CT to perform three-dimensional (3D) imaging of the internal structure of soft tissue engineering scaffolds under compression deformation, as well the nerve tissue engineering scaffolds *in-vivo* [26]. However, this study is limited in terms of the analysis of scaffold structure deformation, and its connection to scaffold mechanical properties.

1.4. Research Issues

Hydrogel scaffolds typically have limited mechanical strength for maintaining the proper support for tissue regeneration [31].Various studies have indicated that the mechanical properties of hydrogel scaffolds, such as their compressive strength and elastic modulus, are typically lower than those of native tissues [6, 32]. This discrepancy poses a significant challenge to their application in tissue engineering, especially when sufficient mechanical strength is crucial.

Usually, scaffolds are expected to simulate the mechanical performance of target tissue, and the requirements on the different applications of scaffolds are expected to be consistent with target tissue [33]. The applications of scaffolds of tissue engineering could be divided into hard tissue and soft tissue. The most notable difference in mechanical properties among various types of tissues and tissue scaffolds lies in their elastic modulus, as depicted in the accompanying diagram [34].

Typically, the elastic modulus of soft tissues falls within the range of 1 to 100 kPa, while hard tissues typically exhibit a significantly higher modulus, exceeding 1000 kPa [35, 36]. Scaffolds for soft tissue have been challenged on characterization of internal architecture.

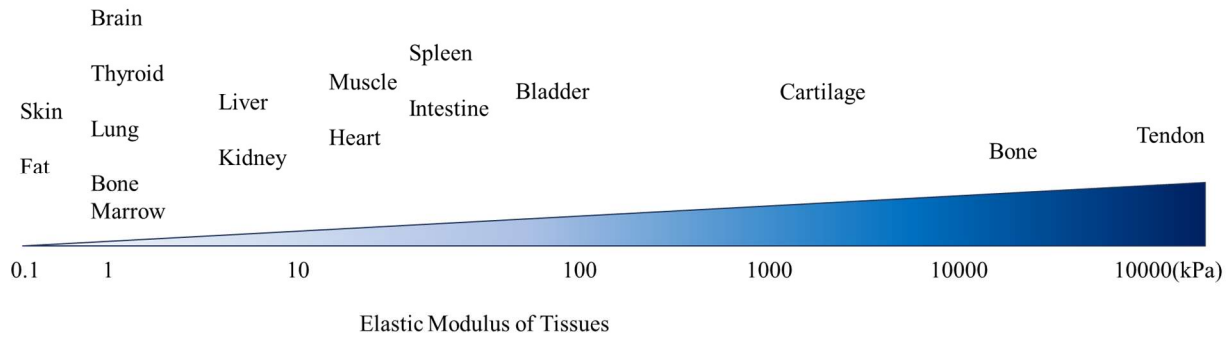

Figure 1.3. elastic modulus of different types of tissue, modified from [34, 35].

Regarding mechanical testing and structural characterization of hard tissue engineering scaffolds, there are currently no significant technical shortcomings in the field of mechanical studies related to these scaffolds. For hard tissue engineering such as bone tissue engineering, cartilage tissue engineering and tendon tissue engineering, the scaffolds for these applications have been characterized on mechanical properties such as modulus and yield strength on compression, stretch, bending and torsion since the mechanical requirements such as elastic modulus and has been thoroughly studied [37-39]. For the hard tissue engineering scaffolds for these uses, usually only slight deformations are expected in the related mechanical environment [18, 40], and scaffolds should have appropriate mechanic modulus to ensure a certain degree of mechanical stimulation to the tissue to induce cell differentiation and proliferation [41]. Given the robust modulus and strength of the scaffolds, their architecture is expected to remain largely undistorted during several hours of μCT scanning [18]. Therefore, the comprehensive evaluation of the internal architecture of scaffolds for hard tissue is not a challenge.

The studies of mechanical properties in soft tissue engineering scaffolds, particularly those based on hydrogels, have been limited in the literature, especially on internal structural deformation characterization of hydrogel scaffolds. This is partly due to the fact that soft tissues are anticipated to be deformable, and detecting such deformations using traditional methods like optical

microscopy can be challenging, since removing scaffolds from the mechanical environment before inspection may change the structure [26]. Hydrogel materials, in particular, demonstrate a complex mechanical behavior that complicates predictions of their structure using Finite Element Analysis (FEA) [42-44]. Furthermore, soft tissues and similar materials exhibit complex mechanical performance due to their viscoelastic behavior, in this case traditional mechanical tests may struggle to adequately capture, and DMA may struggle to find suitable testing parameters [45].

Scaffolds for hard and soft tissues have different requirements when it comes to visualization techniques. Micro-computed tomography (μCT) and magnetic resonance imaging (MRI) are commonly employed as 3D imaging methods that provide sufficient depth and resolution for scaffold visualization. While both techniques offer valuable insights, MRI is often constrained in studies involving mechanical aspects due to the requirement of a metal-free imaging chamber. This limitation can significantly impede the development of research related to scaffold testing and characterization, given that most testing instruments incorporate metallic components. In contrast, μCT is frequently favored in such studies, such as the examination of 3D printed polycaprolactone (PCL)-based scaffolds for bone tissue engineering, despite its longer scanning times, which can extend to several hours [18]. But the long scanning tine is not suitable for studies involving soft tissues, since the long-time consumption for μCT scanning can eventually increase the chance of introducing motion artifact into imaging due to the deformation of soft tissue and scaffolds. And the most critical challenge in conventional absorption-based μCT is to visualize low-density materials due to the low X-ray absorption attenuation of these materials, including hydrogel [26, 27].

Consequently, a comprehensive mechanical characterization method that encompasses both mechanical testing and deformation inspection to facilitate the advancement of soft tissue engineering scaffolds is needed. Conventional visualization techniques are challenged on imaging large depth of architecture of hydrogel scaffolds in mechanical environment. Therefore, to facilitate related research, it is crucial to employ an imaging technique capable of exploring the substantial depths of hydrogel scaffolds with acceptable resolution and speed.

In the previous work from our group [26], a preliminary imaging and analysis of internal structures under compression loading have been carried out, demonstrating the great feasibility of applying SR-PBI-CT on internal micro-structure visualization of hydrogel scaffolds. However, in this previous study, deformation characterization of internal architecture based on imaging is limited with only volume and angle distribution change, importantly leaving to be desired in terms of characterizing the mechanical properties of scaffolds based on their volume data.

1.5. Research Aim and Activities

The aim of this research is to develop a novel method to characterize both mechanical properties and architecture of scaffolds based on SR-PBI-CT. The following activities were to be pursued to achieve this aim.

1) To fabricate hydrogel scaffolds from alginate-gelatin biomaterial solution by 3D printing, which are to be used in the following mechanical testing and imaging.
2) To characterize the mechanical properties of scaffolds by conventional compression testing and further obtain the information on the relaxed stress of scaffolds during compression.
3) To characterize architecture of scaffolds during compression by SR-PBI-CT, where the novel method to characterize the mechanical properties of scaffolds is to be developed, along with examining the deformation of architecture as well as evaluating the relaxed hydrogel stress with obtained images and mechanical testing results.

1.6. Organization of Thesis

This thesis consists of four chapters, including this chapter. Each of the four chapters are briefly described below.

The first chapter presents the background and research aim of the present study. A literature review was performed and presented in terms of hydrogel scaffolds in tissue engineering, mechanical characterization techniques of tissue engineering scaffolds, and visualization of

scaffold architecture. Then, the research issue and aim/objectives are discussed, along with the thesis outline.

The second chapter describes the materials and methods used in this study. It includes three sections: materials and methods for hydrogel scaffolds fabrication and degradation, conventional compression test, and SR-PBI-CT set-up and data process. Each section presents the method to be used in order to pursue each activity as presented in Section 1.5.

The third chapter presents the results and discussion of this study, which include those of (1) imaging data processing for structural and mechanical property assessment, (2) fabrication and degradation of hydrogel scaffolds, (3) conventional compression tests on scaffolds, (4) SR-PBI-CT visualization and analysis of scaffolds under compressive strains, and (5) analysis of the stress-strain curves with the imaging information.

The last chapter presents the conclusion and contribution drawn from the presented study, along with the limitations of this study and recommendations for future work in this field.

CHAPTER 2. MATERIAL AND METHODS

2.1. Materials and Methods for Hydrogel Scaffolds Fabrication and Degradation

2.1.1. Materials and Solution Preparation

2.1.1.1. Hydrogel Preparation

Medium-viscosity alginate powder (A2033, Sigma) and gelatin powder (from porcine skin, G1890, Sigma) were exposed under UV light for 90 mins for sterilization. The alginate and gelatin powders were thoroughly dissolved in phosphate-buffered saline (PBS) to prepare 3% alginate mixed with 1% (w/v) gelatin (hereafter Alg-Ge). All hydrogel solutions were prepared in a sterile environment and transferred to a 4 °C fridge and stored for no more than two weeks.

The detailed protocol of preparing Alg-Ge bioink is given below, as well the photo of some process in Figure 2.1:

1) Mix 1.5 g alginate powder and 0.5 g gelatin powder with 50 ml distilled water in a beaker.
2) Place the beaker on a hot plate and stir overnight. The temperature of the hot plate was set at 60 °C and stir speed was set at 120 rpm.
3) Move the solution into a 37 °C incubator for 24 hours to completely dissolve.
4) Expose the bioink under UV light for 90 mins for sterilization, then move the bioink into a 50ml falcon tube for storge in a 4 °C fridge.
5) Expose the bioink under UV light for 90 mins before printing.

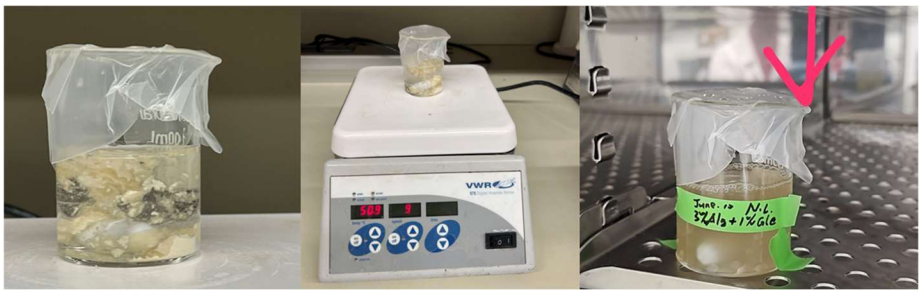

Figure 2.1. Alg-Ge bioink preparation.

2.1.1.2. Crosslinker Preparation

Two kinds of crosslinkers were prepared for the subsequent the printing process: One was prepared by dissolving 50 mM/L calcium chloride in 0.1% polyethyleneimine (PEI; J61270, Alfa Aesar) solution and the other one by dissolving 100 mM/L calcium chloride in distilled water. All solutions were then exposed under UV light for 90 mins for sterilization.

2.1.2. Hydrogel Scaffolds Design and Fabrication

The scaffolds were designed in a cubic shape using Magic 13 Envisiontec software, with the size of 10×10×5 mm^3. Then the cubic file was sliced with the layer height of 160 μm, generated the project file for the control software of the Envision Bioplotter; and the inner structure design was done through the control software of the Envision Bioplotter (VisualMachine software). The infill pattern was the zigzag line and the angle difference between each layer is 90 degrees. The strand distance in each layer is 1.25 mm. The schematic of designed scaffold is shown in Figure 2.2.

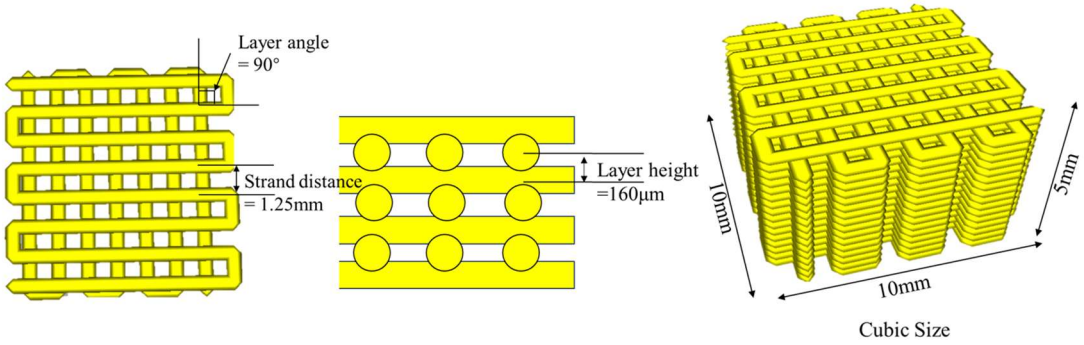

Figure 2.2. Schematic of scaffold design.

Meanwhile, the printed bulks for following material stiffness assessment were also prepared using 3D printing, by changing strand distance to 0.65 mm and keeping all other parameters same, after calculating the volume extrusion speed from imaging data of scaffolds.

The printing of Alg-Ge was carried out using a 3D bioprinter (Envision TEC, Inc., Germany). Prepared hydrogels were, respectively, extruded with air pressures ranging from 10 to 60 kPa over defined time periods at 37 °C. Meanwhile, the movement speed of the printing head can be adjusted within a range of 1 to 30 mm/s. The printing parameters for Alg-Ge were carefully determined through numerous trials, and the optimal settings were found to be an air pressure of 30 kPa and a printing speed of 18 mm/s. Tapered needles with an inner diameter of 200 μm at the outlet (gauge 27, Nordson EFD) were used. The temperature of the printing head and bed were set at 37 °C.

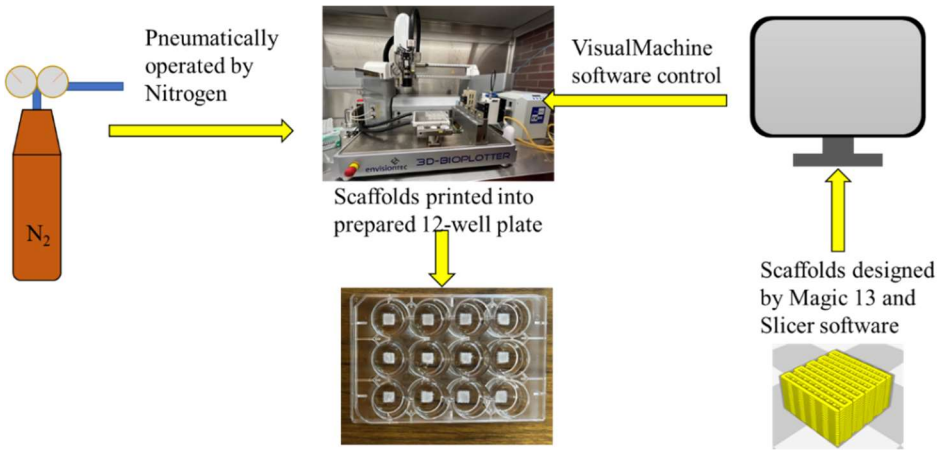

Figure 2.3. Scaffold 3D printing set-up.

Scaffolds were printed using the printing while cross-linking strategy, in which the hydrogel was extruded into the cross-linking medium. Before printing, the well surface (12-well plate) was coated with 0.5% w/v polyethyleneimine (PEI; J61270, Alfa Aesar) and incubated at 37 °C in an incubator for 24 h. After removing the PEI, the plates were rinsed with PBS and each well filled with 2.5 mL of calcium chloride solution, with concentration of 50 mM/L. During the printing process, a constant printing pressure of 30 kPa was applied. The printing head speed was 18 mm/s for Alg-Ge. Five minutes after printing, printed scaffolds were removed from the bottom of well plates and the cross-linking medium was replaced with fresh calcium chloride solution (100 mM/L) and kept at 4 °C for 48 hours to complete cross-linking.

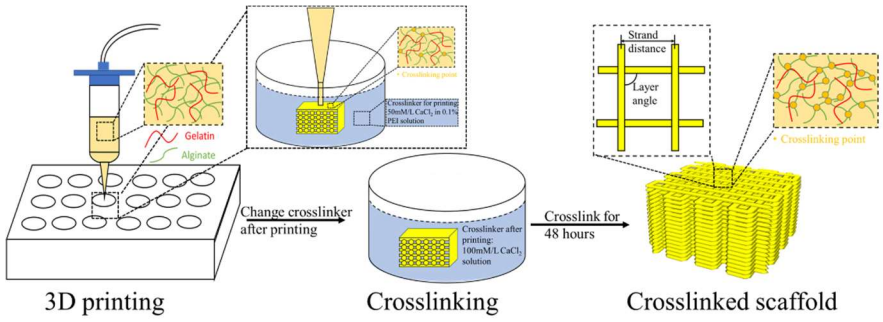

Figure 2.4. Scaffold printing and crosslinking strategy.

2.1.3. *In-vitro* Degradation of Printed Alginate-based Hydrogel Scaffolds

The samples were incubated in 10 mM/L PBS at 37 °C and 5% carbon dioxide for selected degradation periods. The crosslinker was taken out of the samples and the samples were rinsed by PBS, then samples will be soaked in PBS and placed in 37 °C incubator. The ratio of PBS volume to each scaffold was 2 ml/scaffold.

The time point selection of degraded scaffolds in this study is critical for the demonstration of mechanical characterization method. The use of crosslinking of only alginate in bioink can facilitate better control over degradation, particularly when compared to other content crosslinked [46]. The degradation rate of the scaffold can be more precisely regulated when only the alginate is crosslinked. In this study, the scaffolds were considered degraded at the 72-hour mark. By this time point, degraded scaffolds had a significantly change on stiffness, meanwhile can keep the shape for mechanical test and internal architecture imaging.

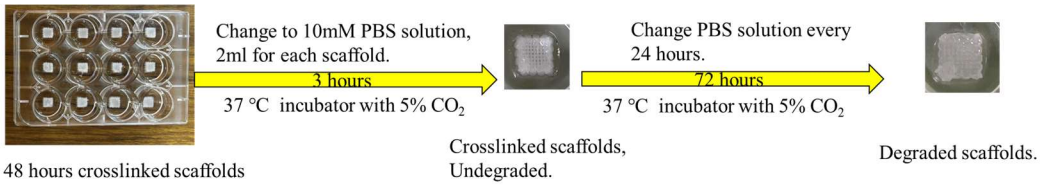

Figure 2.5. *In-vitro* degradation of scaffolds.

2.2. Conventional Stress-strain Characterization of Hydrogel Scaffolds

2.2.1. Compression Test Set-up

Alg-Ge scaffolds with different degradation periods were tested using a compressive testing instrument (Biodynamic System, BOSE) for compression test. Unconfined compression was used for all tests, as shown in Figure 2.6. Before loading the scaffolds, the height of scaffolds and the height after loading were measured by caliper, with the resolution of 0.1mm. The initial height of scaffolds was measured to ensure the scaffolds were not compressed after loading the sample into the testing instrument, meanwhile the readings from the force sensor were double checked to ensure the scaffolds were correctly loaded. After loading each sample, the loaded sample was compressed with a modified loading strategy, as described in the following section. After testing, the testing time, compressive displacement, and compressive force of each sample during test were recorded for stress-strain data processing.

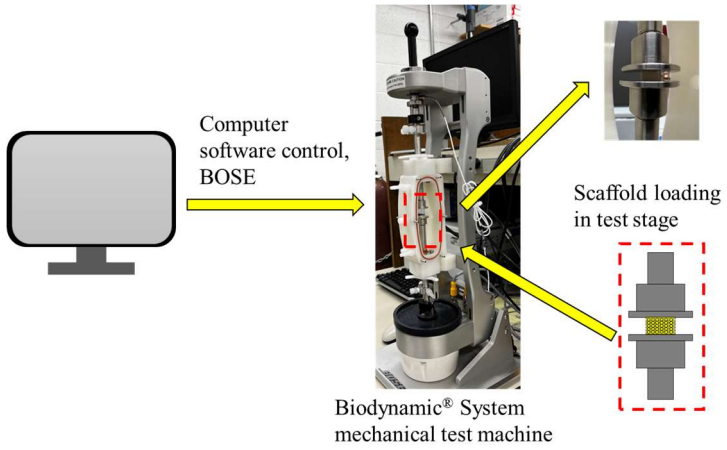

Figure 2.6. Conventional compression test set-up.

2.2.2. Modified Compressive Loading

In this study, compression test was performed with a modified compressive loading on the scaffolds, which was also used on the subsequent imaging of scaffolds. As illustrated Figure. 2.7,

compressive loading was applied to the scaffold sample at a speed of 0.1 mm/s, to reach strains of 10%, 20%, 30%, 40%, and 50%, respectively. Upon reaching each of these strains, the displacement was held for 5 minutes, and the relaxing progress of sample is recorded as the gradually reducing compressive force. The same loading conditions were also applied to the samples of scaffolds which were to be imaged by synchrotron, where during the period of 5 minutes, the imaging and data acquisition took place.

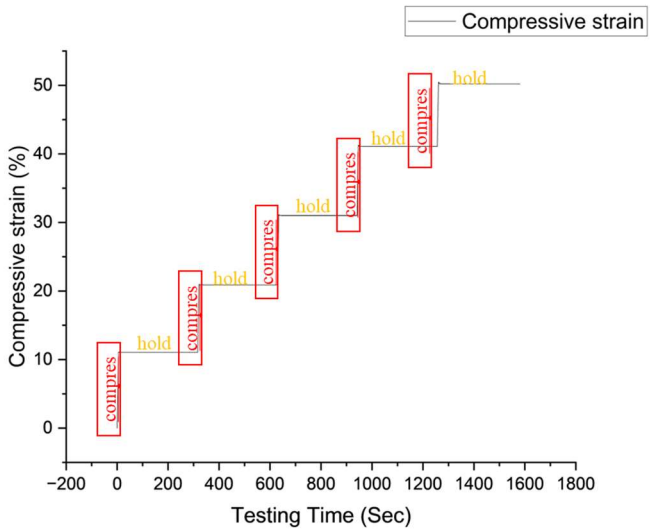

Figure 2.7. Modified compressive strain-time loading plot.

2.2.3. Stress-strain Data Processing

The compressive stress and modulus during imaging period for each group of scaffolds were calculated from the corresponding section of the stress–strain curve, which were obtained from the average value of four compression tests (n = 4) for both undegraded and degraded scaffolds. The detailed method of calculation is presented below.

1) Determine of relaxed compressive force. Relaxed compressive forces were determined with the average value of the force during the last 5 seconds of each “hold” phase of testing.

2) Calculation of cross-sectional area. Cross-sectional areas for mechanical properties calculation are measured differently in this research.

For scaffolds, there are designed and measured values. Designed value was used for conventional evaluation of scaffolds, which was designed outer dimensions; measured values were used for evaluating hydrogel in scaffolds, which were obtained from imaging data, by averaging the area values along the central 10% zone along the vertical direction of each scaffold.

For printed bulks, the cross-sectional area values were measured by conventional method: the length of edge was measured and recorded with a caliper, then side view photos were taken during compression, and edge length was continuously measured by photos. Then the area was calculated as a squire, with measured length. The area calculated by this method should be slightly larger than the actual area since the corners of the printed bulk are rounded.

3) Calculation of stress and modulus. With compressive force and cross-sectional area, stress and modulus were calculated by their definition.

$$Stress = \frac{Force}{Area} \tag{2.1}$$

$$Modulus = \frac{Stress}{Strain} \tag{2.2}$$

2.3. Synchrotron Radiation X-ray Propagation-based Imaging Computed Tomography (SR-PBI-CT) Set-up, Reconstruction, and Imaging Process

2.3.1. Development of Synchrotron Imaging Compressive Retention Device

The study employed the PBI-CT technique to visually examine scaffolds that underwent different levels of compressive strains (Figure 2.8). This technique provided highly accurate 3D data, allowing for a novel perspective that goes beyond traditional mechanical testing. But conventional mechanical test machine is not compatible with synchrotron imaging due to the strong absorption of X-ray beam caused by metal arm.

In order to ensure precise strain measurements, a specialized *in-vitro* X-ray compatible compressive retention device was developed using 3D printing. This device cannot contain metal components in beam and should be able to provide precise compression of hydrogel samples. The device featured a screw-driven piston controlled by a threaded fastener and buoyancy facilitated by PBS within the holder. Meanwhile the device was constructed with no metal material in imaging zone, which ensures the imaging quality of low-density hydrogel material. Precisely fitted square holder and piston ensure uniform compression and zero torsion. The scaffolds were subjected to continuous mechanical stimulation *in-vitro*, resulting in compressive deformation in this study.

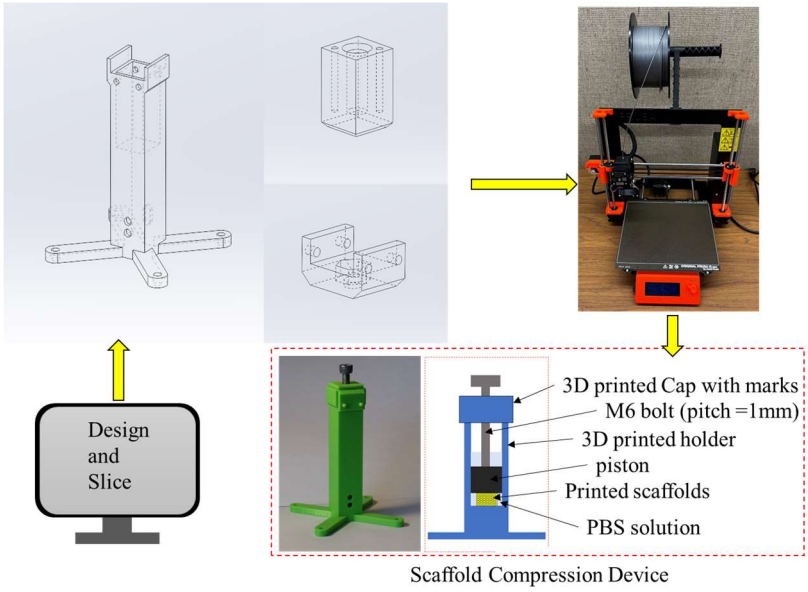

Figure 2.8. Design and manufacture of synchrotron imaging compressive retention device.

2.3.2. SR-PBI-CT Set-up

The PBI method was developed and performed at the 05ID-2 beamline at the biomedical imaging and therapy (BMIT) facility of the Canadian light source (CLS). Samples were imaged at 30 keV and the sample-to-detector distance (SDD) set at 1.5 m. The detector is a beam monitor AA-60 (Hamamatsu Photonics, Shizuoka, Japan) coupled with an ORCA Flash 4.0 camera

(Hamamatsu Photonics, Shizuoka, Japan) with the pixel size of 13× 13 μm^2. The imaging field of view is 26.624 × 9.36 mm^2; 2000 projections over 180° were acquired during a CT scan with an exposure time of 60ms per projection and each scan took about 2 minutes. There was an initial scan with each scaffold loaded, without the compression piston touching the scaffold, and reconstructed images were measured to determine the required displacement of piston to load scaffold at 0% of strain level. Each scaffold (n=3 for each group) was scanned then at its 0, 10%, 20%, 30%, 40%, and 50% compressive strain, respectively, via the specifically designed and manufactured device.

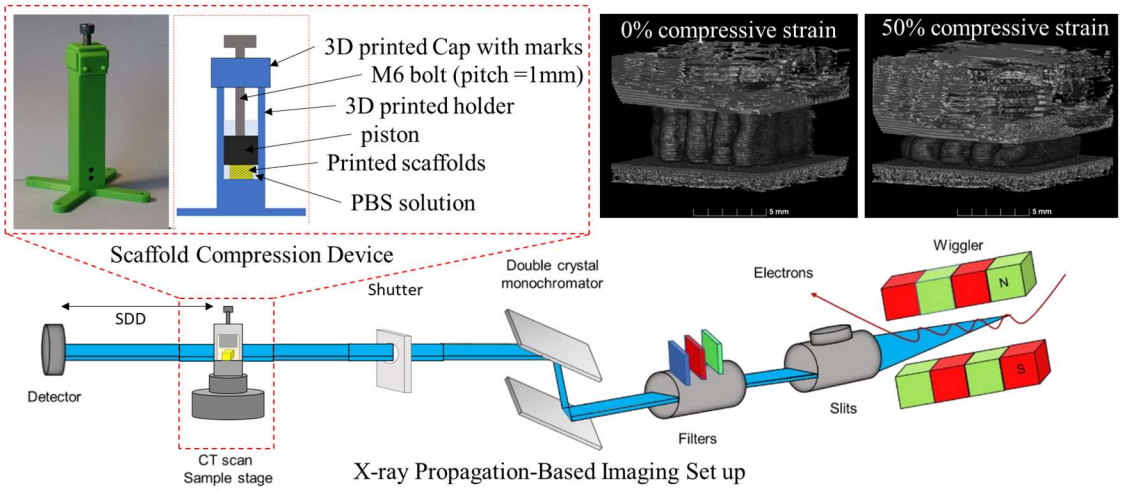

Figure 2.9. SR-PBI-CT set-up.

2.3.3. Reconstruction, Measurements, and Segmentation of Scanned Data

Phase retrieval algorithms were applied to convert edge enhancement phase contrast to areal contrast for further quantitative analysis. An open-source package (the Ultra-Fast-Online, UFO) [47]was used to perform Paganin/transport-of-intensity (TIE) phase retrieval [48] on the projections, followed by CT reconstruction. The 3D volume rendering of the scaffolds was rebuilt with whole cubic block of the printed scaffolds using 3D Slicer. The following data process including 2D measurements and 3D volume segmentation and analysis were done using ImageJ [49], 3D slicer [50], Avizo 2021 (FEI Company) and Biomedisa [51].

2.3.4. Imaging Data Processing for Structural and Mechanical Property Assessment

The degraded and undegraded scaffolds were successfully scanned using the SR-PBI-CT setup, and reconstructed 3D imaging data were processed for mechanical assessment. After visual inspection, the changes on architecture of scaffolds were quantified with precise 3D data. Firstly, the width, height, and cross-section area of strands were measured, by Image J. Then, the volume data and pore size and porosity of scaffolds were measured after volume segmentations done by Avizo and Biomedisa. The detailed flow of processing and calculation is presented below.

1) Measurements of the width, height, and cross-section area of strands by Image J. Geometry properties of strand cross-section view were measured as the following figure, after setting scale with pixel size in Image J.

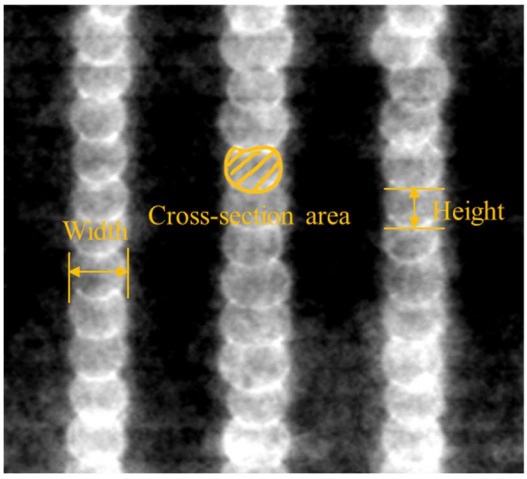

Figure 2.10. Geometry measurements of strands in scaffolds.

2) Volume segmentation by Avizo and Biomedisa. Segmentation of several slices in volume data was manually pre-segmented by Avizo firstly, then the volume data was auto segmented by Biomedisa with pre-segmented label and original image data. There are 3 parts segmented in data, including hydrogel (blue), central pores (yellow), and outer pores (red).

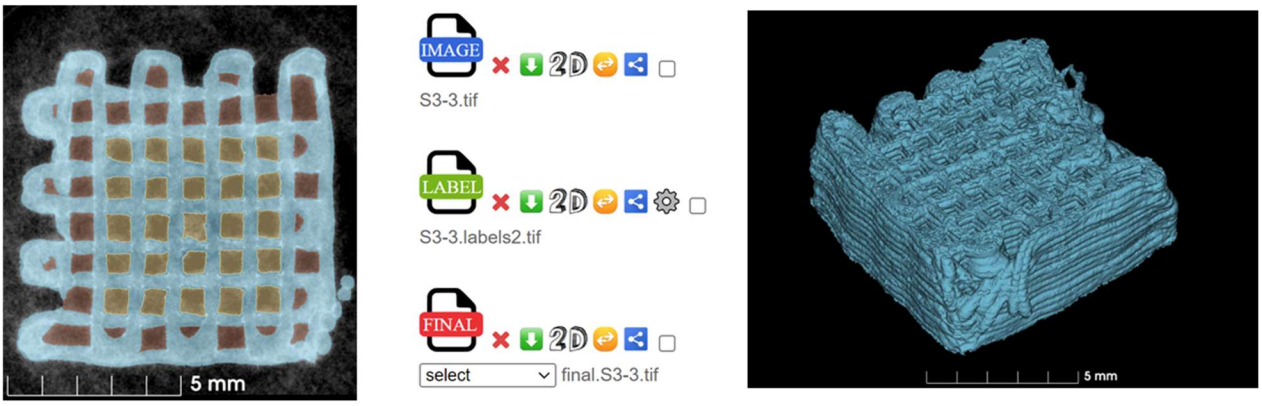

Figure 2.11. Pre-segmentation, Biomedisa auto segmentation, and segmented hydrogel of scaffolds.

3) Calculation of hydrogel volume, porosity, and average pore size. First, segmented data was cropped and 10% height zone of scaffolds on both top and bottom was removed. Then the data was imported into 3D Slicer and volume of 3 parts were obtained from software. Finally, values of cross-sectional area of central pores were obtained in 3D slicer by percentage in height. Then, porosity and average pore size were calculated with following equations:

$$Porosity = \frac{V_{central\ pores} + V_{outer\ pores}}{V_{central\ pores} + V_{outer\ pores} + V_{hydrogel}} \quad (2.3)$$

$$Average\ Pore\ Size = \frac{Average(Area_{\text{central pores}})}{n}, n = 25. \quad (2.4)$$

2.4. Quantification and Statistical Analysis

All experiments were conducted in 3 repeats (for imaging results) or 4 repeats (for compression test) and the data were presented as the average value ± standard deviation. Statistical analysis was conducted using one-way ANOVA on the results. P values <0.05 were considered as statistically different and were marked in the plots using *.

CHAPTER 3. RESULTS AND DISCUSSION

3.1. Conventional Compression Tests on Scaffolds

The applied stress was successfully determined with the modified compression test. The stress-time curves derived from the modified conventional test reveal the typical viscoelastic behavior of hydrogel scaffolds as shown in Figure 3.1.b. Peaks in applied stress were observed during the compression phase of testing, whereas a gradual reduction in stress was evident during relaxation phase when maintaining the compressive strain. Stress values of scaffolds were determined using average relaxed stress values recorded in the final 5 seconds of the imaging period. The stiffness of undegraded and degraded scaffolds were evaluated by computing relaxed Young's modulus at varying strains for each group. Notably, degraded scaffolds exhibited distinct patterns compared to undegraded samples in the compression test. Specifically, degraded scaffolds displayed a higher modulus at lower compressive strains and softening at higher compressive strains (Figure 3.1.c). The compressive force applied, deriving by simulating the mechanical environment of scaffolds during visualization, could serve as a reference of future mechanical analysis.

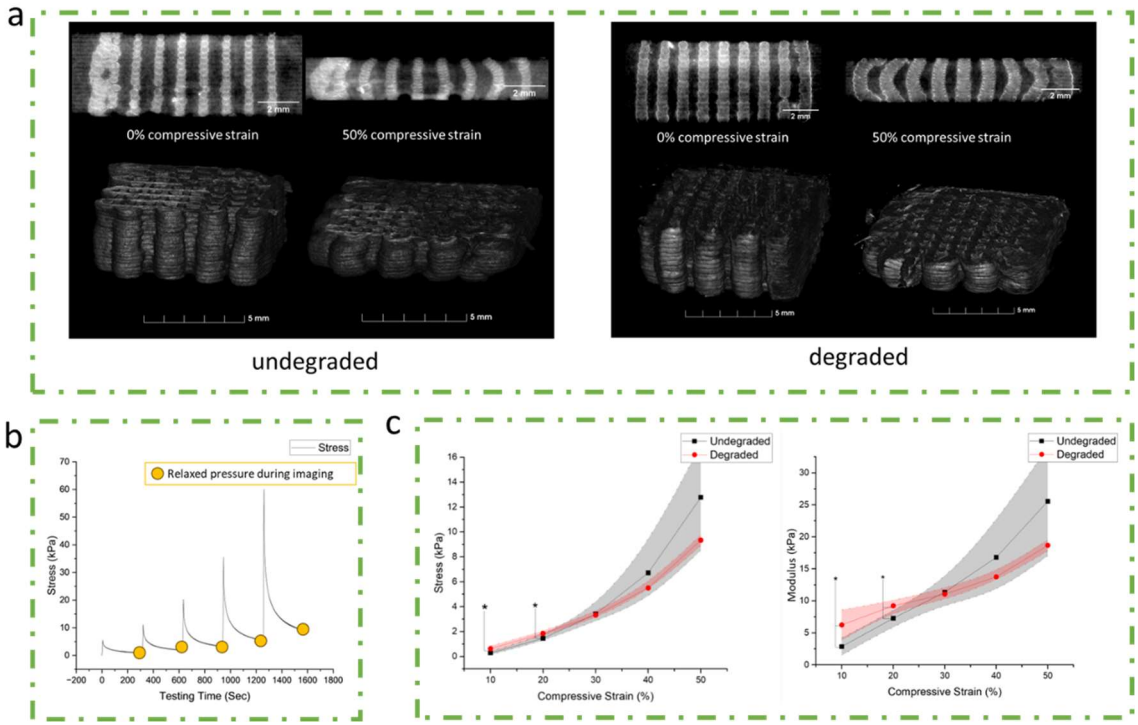

Figure 3.1. Conventional compression test of undegraded and degraded scaffolds. Volume rendering and longitudinal perspective of 2 groups of scaffolds before and after compression (a). Calculation strategy of relaxed stress. Sample of tested stress during compression test, with calculating zone of relaxed stress marked (b). Calculated stress and modulus of degraded and undegraded scaffolds (n=4) (c). *, $p<0.05$.

The fabricated scaffolds have similar elastic modulus to soft tissues and scaffolds with similar material from literatures. The undegraded scaffolds shown nonlinear elastic behavior, and the modulus ranged between around 5-25 kPa, which is within the range of soft tissues such as kidney, heart, muscle, and liver [34, 35]. As well, these scaffolds shown a similar elastic modulus to the literature with similar alginate-based hydrogel scaffolds, such as 3% alginate scaffolds ranged from 15.47-32.1 kPa [33], and 22 kPa for indirect printed 3% alginate scaffolds [52]. Furthermore, for

the printed scaffolds with same Alg-Ge hydrogel material and similar structures, similar modulus and nonlinear elastic behavior with a previous publication were observed [26].

3.2. Fabrication and Degradation of Hydrogel Scaffolds

Undegraded and degraded printed scaffolds with the same internal architecture were successfully prepared and imaged using Alg-Ge solution. The geometric change caused by swelling and degradation was determined using precise 3D data. Firstly, volume rendering and slices from 2 perspectives were performed of undegraded and degraded scaffolds (Figure 3.2.a.). The reconstructed slices showed great image quality and easily to distinguish the scaffold from its background, which indicated the feasibility of SR-PBI-CT technique to visualize low-dense hydrogel scaffolds. Imaging results showed that the scaffolds were printed following the designed pattern and strand distance. Then, the width, height, and cross-section area of strands were determined (Figure 3.2.b.). There were significantly increase on width and cross-section area of the scaffolds with degradation and swelling, mean while there was almost none change on height of strands. Finally, the volume data of scaffolds was measured after volume segmentations done by Avizo and Biomedisa (Figure 3.2.c.). The volume of hydrogel in scaffolds increased, pore size and porosity decreased during degradation and swelling.

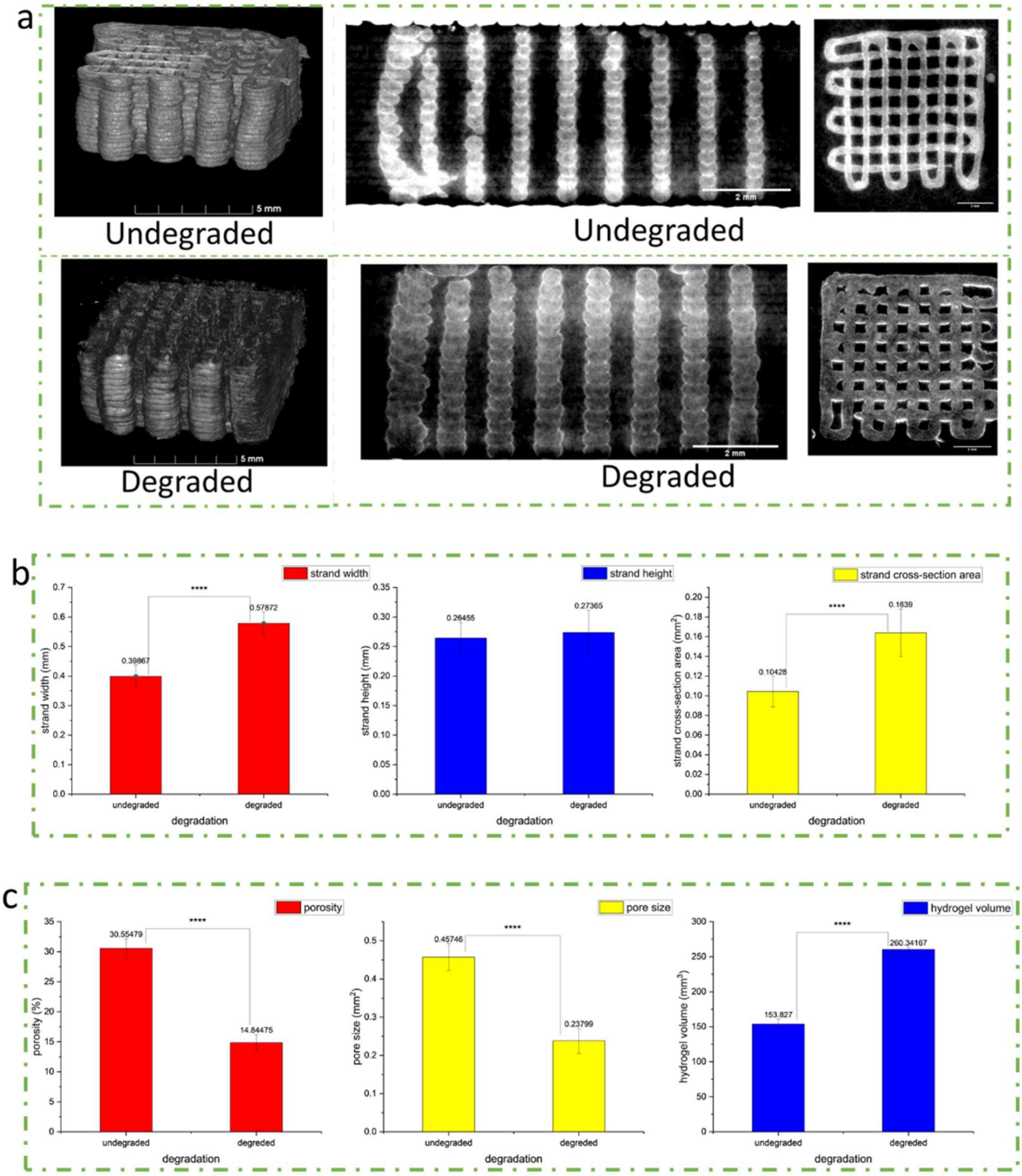

Figure.3.2. Hydrogel scaffolds fabrication and visualization with degraded and undegraded samples. Volume rendering and slices from 2 perspectives of undegraded and degraded scaffolds

(a). Geometric change measurements of strands in undegraded and degraded scaffolds (n=3 for each group), strands were randomly picked from 4 slices in 2 directions of longitudinal view of each scaffold, and 5 strands were randomly picked from each slice (b). Porosity, average pore size and hydrogel volume change during swelling and degradation (n=3), counted with the 80% height range in the middle of the entire scaffolds (c). *, $p<0.05$; **, $p<0.01$; ***, $p<0.005$; ****, $p<0.0005$.

3.3. SR-PBI-CT Visualization and Analysis of Scaffolds under Compressive Strains

The stability of structure was assessed by monitoring changes in the angle distribution of strands. This distribution was quantified based on positional shifts of the strands during compression (Figure 3.3.a). For this analysis, the base layer of strands was chosen as a reference. The angle distribution of subsequent layers relative to the base layer was then determined. During the compression process, the center of the scaffolds bulged outward, altering the overall angle distribution. This alternation was more pronounced in degraded scaffolds. Regarding the value of angle distribution change during compression, both the values and standard deviations of degraded scaffolds increased. This suggests a reduction in structure stability due to swelling and degradation.

Then, changes in the width, height, and cross-sectional area of the strands in both degraded and undegraded scaffolds during compression were measured and analyzed (Figure 3.3.b). All the data showed a clear trend in changing. To be specific, the width expanded, and cross-sectional area decreased during compression. However, the height reduction of strands closely followed the compressive strain.

Pore properties, encompassing pore size and porosity, were then examined (Figure 3.3.c). Different segmentations based on precise CT reconstructed slices were generated to separate the hydrogel and pore, then the volume and cross-sectional area from the segmented reconstructed three-dimensional data were directly counted. On this basis, the volume of pore and hydrogel from segmentations were used to calculate the value of porosity, and pore area from each segmented

slice was used to determine the average pore size of scaffolds. During compression, there was a decline in porosity, pore size, and volume of hydrogel.

After measuring of these deformations, values of strands cross-section area, average pore size and hydrogel volume during compression were normalized and depicted in Figure 3.3.d. The changes in strands cross-section area were consistent, but the degraded scaffolds showed a rapid decrease with increased compression. A more significant reduction was observed in average pore size, whereas the decrease in hydrogel volume was less pronounced during compression. In summary, degraded scaffolds exhibited a more substantial horizontal geometry shift, especially in strands cross-section area and average pore size. Conversely, the reduction in hydrogel volume in degraded scaffolds was relatively minor.

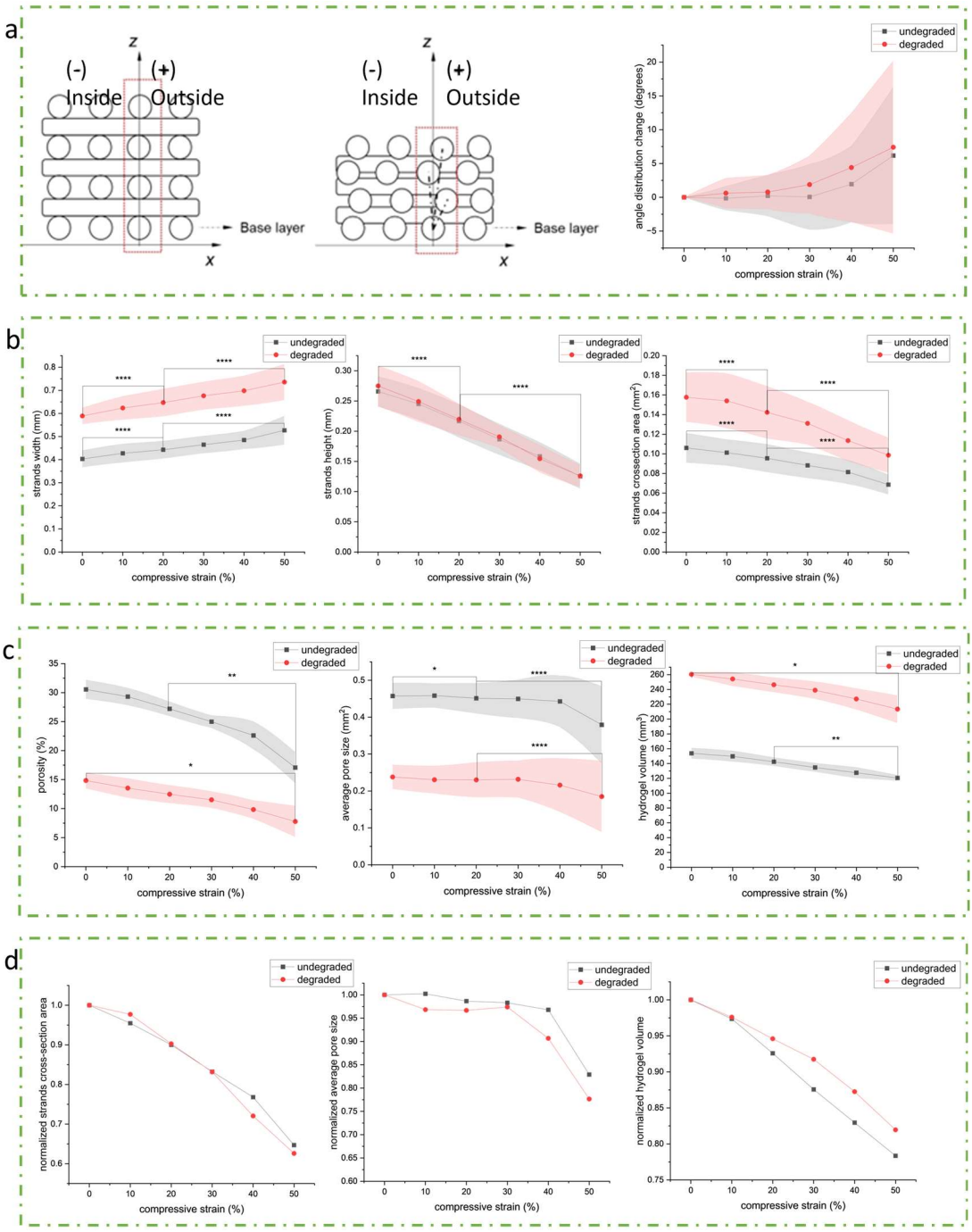

Figure 3.3. PBI-CT visualization and analysis of scaffolds under different compressive strains. Measurement scheme and result of angle distribution change of undegraded and degraded scaffolds

during compression (a). Geometric change measurements of strands in undegraded and degraded scaffolds (n=3) during compression, strands were randomly picked from 4 slices in 2 directions of longitudinal view of each scaffold, and 5 strands were randomly picked from each slice (b). Porosity, average pore size and hydrogel volume change during compression of undegraded and degraded scaffolds (n=3), statistics are made on the 80% height range in the middle of the scaffolds (c). Normalized strands cross-section area, average pore size and hydrogel volume during compression (d). *, $p<0.05$; **, $p<0.01$; ***, $p<0.005$; ****, $p<0.0005$.

3.4. Analysis of the Stress-strain Curves with the Imaging Information

With the information from the scaffold images, the average stresses within the hydrogel of scaffolds (both with and without degradation) were evaluated. First, the compressive forces exerted during the compression were determined from the conventional tests as described above, under the assumption that the forces applied to the scaffolds were identical given that the same loading conditions were applied to the scaffolds in both compression testing and imaging. Then, the cross-sectional area of the hydrogel was calculated, based on the imaging information, by averaging the area values within the central zone with a height of 10% of entire scaffold height along the vertical direction. After that, the average stress values were derived from the above forces and cross-sectional area, with the result shown in Figure 3.4.a. On this basis, the module was also evaluated with the results presented in Figure 3.4.b. It is evident that both undegraded and degraded scaffolds exhibit a similar trend during compressive strain up to 30%, which is different with the result when cross-sectional area is not considered (Figure 3.4.c). However, the stress within the hydrogel of undegraded scaffolds increases rapidly during compression. At 50% strain, the stress reached a significant difference between undegraded and degraded scaffolds, while the relaxed compressive forces were similar, respectively. It is apparent that the differences in hydrogel stress are more pronounced than the variances in compressive force.

Meanwhile, the precision of this method is successfully verified with the comparison with the conventional mechanical test results from a set of printed bulk samples. Relaxed stress and Young's

modulus of hydrogel within undegraded scaffolds and printed bulks were similar (Figure 3.4.b), considering the cross-sectional area of bulk was calculated slightly larger comparing with actual area using conventional method, leading to a smaller stress and modulus comparing with actual values. The similarity demonstrated the precision of this combined method to access the stress within hydrogel of the scaffolds.

Following this method, the average stress within the hydrogel of undegraded and degraded scaffolds was available. This comprehensive analysis provides valuable insights into the mechanical behavior and performance of the scaffolds, contributing to the understanding of their potential applications in various fields, such as tissue engineering and regenerative medicine.

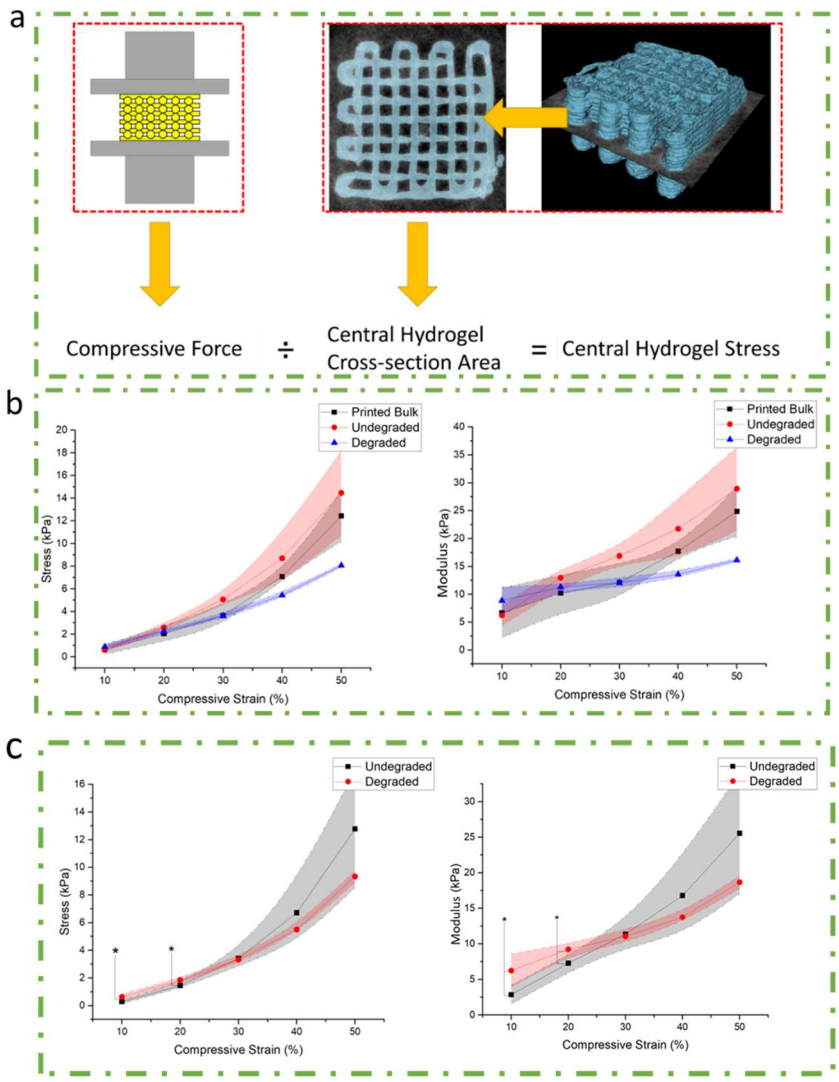

Figure 3.4. Average stress in hydrogel of both undegraded and degraded scaffolds. Calculation scheme of average central hydrogel stress (a). Calculated average stress and modulus in hydrogel during compression using imaging data, with printed undegraded bulk sample (b). Calculated stress and modulus of degraded and undegraded scaffolds without imaging data (n=4) (c). *, $p<0.05$.

CHAPTER 4. CONCLUSIONS AND RECOMMENDATIONS

4.1. Summary and Conclusions

Non-invasive characterization of 3D bio printed hydrogel scaffolds in physical environment is critical for facilitating longitude studies on tissue engineering scaffolds. In this research, a novel mechanical characterization method on hydrogel scaffolds was developed based on conventional compression test and SR-PBI-CT technique. This method is demonstrated with three parts of research after successfully preparing samples: First, modified conventional compression tests can determine the stress of hydrogel scaffolds in mechanical environments during visualization; then 3D volume data from SR-PBI-CT imaging can be used for detailed analysis of internal architecture of scaffolds; finally, the combination of the result from modified compression test and SR-PBI-CT imaging can provide the further characterization of mechanical properties of scaffolds with precision in mechanical environment.

First, developed compression tests successfully determined the relaxed stress of hydrogel scaffolds in mechanical environments during visualization. The modified conventional strain-time loading strategy can ensure the mechanical environment of scaffolds were consistent in this study, and typical stress-time curves showing viscoelastic properties of hydrogel were obtained. With the mechanical reaction of scaffolds under specific mechanical environment recorded, the relaxed stress was obtained as applied stress for future analysis, with the range around 5-25 kPa. Two groups of samples showed significantly different results within the 20% range of compressive strain.

Then 3D volume data from SR-PBI-CT images can be used to examine the internal architecture of scaffolds. The structure stability, geometry change of strands, and changes in the properties of pore were successfully characterized using reconstructed 3D data. Characterization of internal architecture of scaffolds was successfully demonstrated.

Finally, the combination of the result from modified compression test and SR-PBI-CT imaging can provide the further characterization of mechanical property of scaffolds in mechanical

environment with verified precision. The stress in hydrogel material of scaffolds was calculated with the compressive force and hydrogel cross-sectional area, determined average max stress as 14kPa for undegraded scaffolds and 8 kPa for degraded scaffolds. Furthermore, the precision of the method has been successfully verified by comparing results of undegraded scaffolds and conventional tested undegraded printed bulk.

This research reveals the great potential of applying SR-PBI-CT to monitor and characterize the bio-hydrogel scaffolds non-invasively in mechanical environments of tissue engineering. The results from this study have illustrated that the mechanical properties and microstructures of scaffolds, whether being degraded or not, can be examined and characterized by the SR-PBI-CT imaging, in a non-destructive manner. This would represent a significant advance for facilitating longitude studies on the scaffolds, once implanting them in animal model or human patient with more complicated mechanical environment.

4.2. Limitations and Recommendations

The limitations of the presented study are listed and discussed below, along with the recommendations to expand this method into tissue engineering application.

1) The mechanical tests were conducted separately from the imaging process. In this study, the imaging stage didn't incorporate the mechanical test, potentially leading to imprecision when applying mechanical loading to the tested samples. For future research, the development of an advanced testing device that can remotely offer *in-situ* mechanical loading and testing during imaging process is suggested. This would significantly enhance the precision and convenience of mechanical characterization of hydrogel scaffolds.
2) For conventional compression test, a 5-minute observation period proves insufficient to comprehensively analyze the relaxation behavior exhibited by hydrogel scaffolds. Moreover, when attempting to monitor the behavior at a 50% strain level, the relaxation process does not reach equilibrium within this limited timeframe. Consequently, future research focused

on determining the relaxed modulus of hydrogel scaffolds will necessitate an extended monitoring period in order to ensure that relaxation reaches equilibrium at various selected strain levels.

3) In this study, the complex viscoelastic behavior of hydrogel scaffolds is not addressed. Instead, relaxed stress was employed for mechanical characterization of hydrogel scaffolds. Typically, the viscoelastic behavior of hydrogel material is usually described by storge and loss moduli, which are assessed using rheometers or dynamic mechanical analyzers. While dynamic mechanical analysis is suitable for evaluating hydrogel scaffolds, specific testing parameters, such as vibrating frequency and strain, must be validated for varied tissue engineering applications. Future research could include this aspect and characterize the scaffolds viscoelastic behaviors for the unique needs with specific mechanical environments of target tissues.

4) The mechanical stimulate in this study is compression only. However, the actual mechanical conditions of tissue engineering scaffolds could be more diverse, encompassing torsion, bending, compression and tensile forces. For future study, it could be valuable to develop a set of methods that can accurately capture and replicate the complex mechanical environment specific to the target tissue.

5) The reconstruction and segmentation algorithms aren't fully compatible, leading to blurred imaging and occasional inaccuracies in scaffold segmentation. The reconstructed slices display inconsistent background grey scale across different parts of scaffolds, and random bright spots appear in slices. These inconsistencies complicate manual pre-segmentation. It is essential to develop a more effective reconstruction algorithm to improve the segmentation of hydrogel scaffolds, for both *in-vitro* and *in-vivo* future studies.

REFERENCES.

[1] S. J. Hollister, "Porous scaffold design for tissue engineering," *Nature materials,* vol. 4, no. 7, pp. 518-524, 2005.

[2] Q. L. Loh and C. Choong, "Three-dimensional scaffolds for tissue engineering applications: role of porosity and pore size," 2013.

[3] P. X. Ma, "Scaffolds for tissue fabrication," *Materials today,* vol. 7, no. 5, pp. 30-40, 2004.

[4] D. X. Chen, *Extrusion Bioprinting of Scaffolds* (Extrusion Bioprinting of Scaffolds for Tissue Engineering Applications). Springer, 2019.

[5] W. E. Hennink and C. F. van Nostrum, "Novel crosslinking methods to design hydrogels," *Advanced drug delivery reviews,* vol. 64, pp. 223-236, 2012.

[6] M. W. Tibbitt and K. S. Anseth, "Hydrogels as extracellular matrix mimics for 3D cell culture," *Biotechnology and bioengineering,* vol. 103, no. 4, pp. 655-663, 2009.

[7] B. K. Singh, R. Sirohi, D. Archana, A. Jain, and P. Dutta, "Porous chitosan scaffolds: a systematic study for choice of crosslinker and growth factor incorporation," *International Journal of Polymeric Materials and Polymeric Biomaterials,* vol. 64, no. 5, pp. 242-252, 2015.

[8] Y. S. Zhang and A. Khademhosseini, "Advances in engineering hydrogels," *Science,* vol. 356, no. 6337, p. eaaf3627, 2017.

[9] C. Larson and R. Shepherd, "3D bioprinting technologies for cellular engineering," in *Microscale Technologies for Cell Engineering*: Springer, 2016, pp. 69-89.

[10] D. E. Discher, P. Janmey, and Y.-l. Wang, "Tissue cells feel and respond to the stiffness of their substrate," *Science,* vol. 310, no. 5751, pp. 1139-1143, 2005.

[11] B. Derby, "Printing and prototyping of tissues and scaffolds," *science,* vol. 338, no. 6109, pp. 921-926, 2012.

[12] M. M. Martino *et al.*, "Growth factors engineered for super-affinity to the extracellular matrix enhance tissue healing," *Science,* vol. 343, no. 6173, pp. 885-888, 2014.

[13] H. H. Lu and S. Thomopoulos, "Functional attachment of soft tissues to bone: development, healing, and tissue engineering," *Annual review of biomedical engineering,* vol. 15, pp. 201-226, 2013.

[14] W. Brostow, "Dynamic Mechanical Analysis: a practical introduction," ed: CRC Press, USA, 2007.

[15] D. Dunson, "Characterization of polymers using dynamic mechanical analysis (DMA)," *EAG Appl Note,* 2017.

[16] V. Karageorgiou and D. Kaplan, "Porosity of 3D biomaterial scaffolds and osteogenesis," *Biomaterials,* vol. 26, no. 27, pp. 5474-5491, 2005.

[17] A. A. Zadpoor, "Mechanical performance of additively manufactured meta-biomaterials," *Acta biomaterialia,* vol. 85, pp. 41-59, 2019.

[18] J. N. Clark *et al.*, "Exploratory Full-Field Mechanical Analysis across the Osteochondral Tissue—Biomaterial Interface in an Ovine Model," *Materials,* vol. 13, no. 18, p. 3911, 2020.

[19] X. Liu, K. Tobita, R. J. Francis, and C. W. Lo, "Imaging techniques for visualizing and phenotyping congenital heart defects in murine models," *Birth Defects Research Part C: Embryo Today: Reviews,* vol. 99, no. 2, pp. 93-105, 2013.

[20] A. Woesz *et al.*, "Towards bone replacement materials from calcium phosphates via rapid prototyping and ceramic gelcasting," *Materials Science and Engineering: C,* vol. 25, no. 2, pp. 181-186, 2005.

[21] S. K. Hedayati, A. H. Behravesh, S. Hasannia, A. B. Saed, and B. Akhoundi, "3D printed PCL scaffold reinforced with continuous biodegradable fiber yarn: A study on mechanical and cell viability properties," *Polymer Testing,* vol. 83, p. 106347, 2020.

[22] D. W. Hutmacher, "Scaffold design and fabrication technologies for engineering tissues—state of the art and future perspectives," *Journal of Biomaterials Science, Polymer Edition,* vol. 12, no. 1, pp. 107-124, 2001.

[23] B. D. Ratner, A. S. Hoffman, F. J. Schoen, and J. E. Lemons, *Biomaterials science: an introduction to materials in medicine*. Elsevier, 2004.

[24] I. F. Cengiz, J. M. Oliveira, and R. L. Reis, "Micro-CT–a digital 3D microstructural voyage into scaffolds: a systematic review of the reported methods and results," *Biomaterials research,* vol. 22, pp. 1-11, 2018.

[25] J. D. Boerckel, D. E. Mason, A. M. McDermott, and E. Alsberg, "Microcomputed tomography: approaches and applications in bioengineering," *Stem cell research & therapy,* vol. 5, no. 6, pp. 1-12, 2014.

[26] L. Ning *et al.*, "Noninvasive Three-Dimensional In Situ and In Vivo Characterization of Bioprinted Hydrogel Scaffolds Using the X-ray Propagation-Based Imaging Technique," *ACS Applied Materials & Interfaces,* 2021.

[27] X. Duan, N. Li, X. Chen, and N. Zhu, "Characterization of tissue scaffolds using synchrotron radiation microcomputed tomography imaging," *Tissue Engineering Part C: Methods,* vol. 27, no. 11, pp. 573-588, 2021.

[28] R. A. Lewis, "Medical phase contrast x-ray imaging: current status and future prospects," *Physics in medicine & biology,* vol. 49, no. 16, p. 3573, 2004.

[29] Z. Izadifar, A. Honaramooz, S. Wiebe, G. Belev, X. Chen, and D. Chapman, "Low-dose phase-based X-ray imaging techniques for in situ soft tissue engineering assessments," *Biomaterials,* vol. 82, pp. 151-167, 2016.

[30] M. Nair, J. H. Shepherd, S. M. Best, and R. E. Cameron, "MicroCT analysis of connectivity in porous structures: optimizing data acquisition and analytical methods in the context of tissue engineering," *Journal of the Royal Society Interface,* vol. 17, no. 165, p. 20190833, 2020.

[31] S. Naghieh, M. R. Karamooz-Ravari, M. Sarker, E. Karki, and X. Chen, "Influence of crosslinking on the mechanical behavior of 3D printed alginate scaffolds: Experimental and numerical approaches," *J. Mech. Behav. Biomed. Mater.,* vol. 80, pp. 111-118, 2018.

[32] J. P. Gong, "Why are double network hydrogels so tough?," *Soft Matter,* vol. 6, no. 12, pp. 2583-2590, 2010.

[33] S. Naghieh, M. Sarker, M. R. Karamooz-Ravari, A. D. McInnes, and X. Chen, "Modeling of the mechanical behavior of 3D bioplotted scaffolds considering the penetration in interlocked strands," *Applied Sciences,* vol. 8, no. 9, p. 1422, 2018.

[34] A. M. Handorf, Y. Zhou, M. A. Halanski, and W.-J. Li, "Tissue stiffness dictates development, homeostasis, and disease progression," *Organogenesis,* vol. 11, no. 1, pp. 1-15, 2015.

[35] I. M. Lei *et al.*, "3D printed biomimetic cochleae and machine learning co-modelling provides clinical informatics for cochlear implant patients," *Nature Communications,* vol. 12, no. 1, p. 6260, 2021.

[36] T. R. Cox and J. T. Erler, "Remodeling and homeostasis of the extracellular matrix: implications for fibrotic diseases and cancer," *Disease models & mechanisms,* vol. 4, no. 2, pp. 165-178, 2011.

[37] F. You, B. F. Eames, and X. Chen, "Application of extrusion-based hydrogel bioprinting for cartilage tissue engineering," *International journal of molecular sciences,* vol. 18, no. 7, p. 1597, 2017.

[38] Q. Fu, E. Saiz, M. N. Rahaman, and A. P. Tomsia, "Bioactive glass scaffolds for bone tissue engineering: state of the art and future perspectives," *Materials Science and Engineering: C,* vol. 31, no. 7, pp. 1245-1256, 2011.

[39] C. Rinoldi *et al.*, "Mechanical and biochemical stimulation of 3D multilayered scaffolds for tendon tissue engineering," *ACS Biomaterials Science & Engineering,* vol. 5, no. 6, pp. 2953-2964, 2019.

[40] A. Dhillon *et al.*, "Analysis of sintered polymer scaffolds using concomitant synchrotron computed tomography and in situ mechanical testing," *Journal of Materials Science: Materials in Medicine,* vol. 22, no. 12, pp. 2599-2605, 2011.

[41] A. A. Al-Tamimi, P. R. A. Fernandes, C. Peach, G. Cooper, C. Diver, and P. J. Bartolo, "Metallic bone fixation implants: A novel design approach for reducing the stress shielding phenomenon," *Virtual and Physical Prototyping,* vol. 12, no. 2, pp. 141-151, 2017.

[42] R. Hedayati, M. Sadighi, M. Mohammadi-Aghdam, and A. Zadpoor, "Mechanical behavior of additively manufactured porous biomaterials made from truncated cuboctahedron unit cells," *International Journal of Mechanical Sciences,* vol. 106, pp. 19-38, 2016.

[43] Y. Leng, V. Tac, S. Calve, and A. B. Tepole, "Predicting the mechanical properties of biopolymer gels using neural networks trained on discrete fiber network data," *Computer Methods in Applied Mechanics and Engineering,* vol. 387, p. 114160, 2021.

[44] F. Yang, D. Das, K. Karunakaran, G. M. Genin, S. Thomopoulos, and I. Chasiotis, "Nonlinear time-dependent mechanical behavior of mammalian collagen fibrils," *Acta Biomaterialia,* vol. 163, pp. 63-77, 2023.

[45] D. Chimene, R. Kaunas, and A. K. Gaharwar, "Hydrogel bioink reinforcement for additive manufacturing: a focused review of emerging strategies," *Advanced materials,* vol. 32, no. 1, p. 1902026, 2020.

[46] Y. Luo, T. Zhang, and X. Lin, "3D printed hydrogel scaffolds with macro pores and interconnected microchannel networks for tissue engineering vascularization," *Chemical Engineering Journal,* vol. 430, p. 132926, 2022.

[47] M. Vogelgesang *et al.*, "Real-time image-content-based beamline control for smart 4D X-ray imaging," *Journal of synchrotron radiation,* vol. 23, no. 5, pp. 1254-1263, 2016.

[48] D. Paganin, S. C. Mayo, T. E. Gureyev, P. R. Miller, and S. W. Wilkins, "Simultaneous phase and amplitude extraction from a single defocused image of a homogeneous object," *Journal of microscopy,* vol. 206, no. 1, pp. 33-40, 2002.

[49] C. A. Schneider, W. S. Rasband, and K. W. Eliceiri, "NIH Image to ImageJ: 25 years of image analysis," *Nature methods,* vol. 9, no. 7, pp. 671-675, 2012.

[50] R. Kikinis, S. D. Pieper, and K. G. Vosburgh, "3D Slicer: a platform for subject-specific image analysis, visualization, and clinical support," in *Intraoperative imaging and image-guided therapy*: Springer, 2013, pp. 277-289.

[51] P. D. Lösel *et al.*, "Introducing Biomedisa as an open-source online platform for biomedical image segmentation," *Nature communications,* vol. 11, no. 1, p. 5577, 2020.

[52] S. Naghieh, M. Sarker, E. Abelseth, and X. Chen, "Indirect 3D bioprinting and characterization of alginate scaffolds for potential nerve tissue engineering applications," *J. Mech. Behav. Biomed. Mater.,* vol. 93, pp. 183-193, 2019.